NASA/TM—20220000668

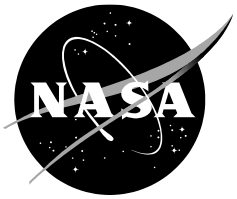

Exploration of an Adaptive Routine for Battery Modeling

Kenneth W. Eure
Langley Research Center, Hampton, Virginia

Edward F. Hogge
National Institute of Aerospace, Hampton, Virginia

March 2022

NASA STI Program Report Series

Since its founding, NASA has been dedicated to the advancement of aeronautics and space science. The NASA scientific and technical information (STI) program plays a key part in helping NASA maintain this important role.

The NASA STI program operates under the auspices of the Agency Chief Information Officer. It collects, organizes, provides for archiving, and disseminates NASA's STI. The NASA STI program provides access to the NTRS Registered and its public interface, the NASA Technical Reports Server, thus providing one of the largest collections of aeronautical and space science STI in the world. Results are published in both non-NASA channels and by NASA in the NASA STI Report Series, which includes the following report types:

- TECHNICAL PUBLICATION. Reports of completed research or a major significant phase of research that present the results of NASA Programs and include extensive data or theoretical analysis. Includes compilations of significant scientific and technical data and information deemed to be of continuing reference value. NASA counterpart of peer-reviewed formal professional papers but has less stringent limitations on manuscript length and extent of graphic presentations.

- TECHNICAL MEMORANDUM. Scientific and technical findings that are preliminary or of specialized interest, e.g., quick release reports, working papers, and bibliographies that contain minimal annotation. Does not contain extensive analysis.

- CONTRACTOR REPORT. Scientific and technical findings by NASA-sponsored contractors and grantees.

- CONFERENCE PUBLICATION. Collected papers from scientific and technical conferences, symposia, seminars, or other meetings sponsored or co-sponsored by NASA.

- SPECIAL PUBLICATION. Scientific, technical, or historical information from NASA programs, projects, and missions, often concerned with subjects having substantial public interest.

- TECHNICAL TRANSLATION. English-language translations of foreign scientific and technical material pertinent to NASA's mission.

Specialized services also include organizing and publishing research results, distributing specialized research announcements and feeds, providing information desk and personal search support, and enabling data exchange services.

For more information about the NASA STI program, see the following:

- Access the NASA STI program home page at http://www.sti.nasa.gov

- Help desk contact information:

https://www.sti.nasa.gov/sti-contact-form/
and select the "General" help request type.

NASA/TM—20220000668

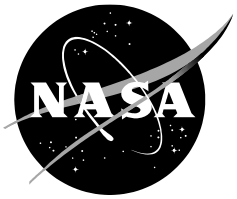

Exploration of an Adaptive Routine for Battery Modeling

Kenneth W. Eure
Langley Research Center, Hampton, Virginia

Edward F. Hogge
National Institute of Aerospace, Hampton, Virginia

National Aeronautics and
Space Administration

Langley Research Center
Hampton, VA 23681-2199

March 2022

Acknowledgments

The authors would like to thank NASA's Aeronautics Research Mission Directorate for its leadership, support, and sponsorship regarding the subject of this report and the System Wide Safety project management of Steven Young.

Special thanks to Chetan Kulkarni on assistance with the battery models and the system Identification process, and to Matt Daigle for the open source battery model code and previous research.

Available from:

NASA STI Program / Mail Stop 148
NASA Langley Research Center
Hampton, VA 23681-2199
Fax: 757-864-6500

Contents

Abstract

The purpose of this document is to explore the use of adaptive routines in battery modeling. The adaptive routines consist of real-time state estimators combined with battery parameter model components that are adjusted in real-time as battery data becomes available. Several aspects are explored. It is shown that model parameter identification is possible for simple battery models using available input/output data measurements. The online system identification used is recursive least squares. Model identification may be combined with a state observer such as the extended Kalman filter or the unscented Kalman filter to form an adaptive model combined with state estimation. However, such a combination is found to be problematic due to uncertainty, observability, and stability issues. This paper is organized as follows. Section 1 introduces adaptive routines and possible roles they play in battery modeling. In Section 2 real-time parameter identification is described with results based on battery data. Section 3 reviews various state estimators and results using a simple battery model. In Section 4 parameter identification and state estimation are combined to form an adaptive routine. Finally, in Section 5 conclusions are drawn and future work is suggested.

1. Introduction

There exists a need to estimate the useable charge of a battery to predict the time to exhaustion under expected load demand. State of Charge (SoC) is an estimate of the internal charge state. Since SoC is not directly measurable, it must be estimated using measurements of battery current and voltage. Several methods to model the dependence of the voltage on the current and battery's internal state include electrochemistry models, equivalent circuit models, and models using some type of input/output mapping such as neural networks. Each type of modeling method has advantages and disadvantages. The electrochemistry model is the most detailed we considered and relates most closely to the battery physics. However, it has the most tuning challenges and is the most complex model and therefore might offer tuning challenges and trouble with robustness. Neural network models could offer accurate input/output mapping but are not suitable for real-time adaptation due to their reliance on a-priori data. The equivalent circuit model is simple, robust, and easily relates basic battery dynamics to a small set of parameters for possible tuning. A disadvantage of the equivalent circuit model is that it is not as accurate as more complex models so the battery state estimates and predictions can be inferior and suffers as the battery's internal parameters shift with battery age. However, this loss of accuracy may be tolerated due to the advantages gained in robustness and potential use in adaptive routines due to the model's mathematical simplicity, intuitive appeal, and ease of accommodation of real-time parameter updates. Both battery parameter estimation and model state observation are obtained through correlation techniques, such as Kalman filtering.

Kalman filtering is an established technology used since the Apollo program [1] for the estimation of states within a dynamic system. For linear systems, this method of state estimation is optimal. The Kalman filter consists of a set of recursive equations that are evaluated repeatedly and updated using input/output measurements as the system operates. The mathematical model of the system consists of two noise sources: process and measurement noise. Process noise is noise in the state estimate due to inaccuracies and model parameter errors. Measurement noise consists of sensor errors and electrical noise. For linear observable systems with known process and measurement noise variances, the Kalman filter has been widely employed as the optimal state estimator. However, many systems are nonlinear. In our case, the battery discharge voltage profile is a nonlinear function of the input

current demand. To approximate an application of the Kalman filter to nonlinear systems, the Extended Kalman Filter (EKF) has been developed. The EKF is derived from the nonlinear system equations by representation of the nonlinear system using the first term of the nonlinear equation's Taylor series expansion. This makes development of the Kalman filter possible for nonlinear systems but sacrifices system representation by employing an approximate (linear) model. For battery modeling, the EKF has been used as a state observer of the underlying nonlinear battery behavior [2].

State observers are used to update battery state estimates of internal state values based on observations of current and voltage at the battery output terminals. An equivalent circuit battery model in [3] [4] is used to represent battery terminal voltage dynamics as a function of battery current. The model is based on Thevenin's theorem used to model the current and voltage profile of the battery as a black box input-output device. A first-approximation assumption is made such that the battery state can match a linear electrical network consisting of only voltage and current sources and resistances and capacitors. Thevenin states that the black box can be replaced at the input output terminals by an equivalent voltage source in series connection with an equivalent resistance and capacitance. The correspondence of the resistor capacitor (RC) circuit to actual battery chemical phenomena is only notional. To extend the equivalent circuit model, some of the components were made to vary according to the bulk charge stored in the battery. The SoC is an estimate of the battery bulk charge. The battery input-output voltage dynamics will change as a function of this bulk charge estimate. Battery SoC is defined as:

$$SoC = \frac{C_t}{C_{Max}} = S_0 - \frac{\int_{t_0}^{t} \eta I(\zeta) d\zeta}{C_{Max}}$$

Where C_t represents the charge stored in the battery, C_{Max} is the maximum charge that the battery can hold. I is the current drawn during discharge, η is the coulombic efficiency assumed to be one, and S_0 is the initial SoC at time t_0. ζ is a dummy variable of integration.

Model-based battery SoC estimation has been developed here using an equivalent circuit representation [3]. The equivalent circuit model is chosen due to its simplicity, robustness, and ability to be formulated into a linear representation for adaptive linear techniques such as recursive least squares. Various methods of performance analyses and conditions under which the model state is observable have been proposed and demonstrated using simulated and experimental battery data [5]. The EKF has been analyzed and demonstrated in tutorials including detail development and discussion [2]. In addition to the EKF, the Unscented Kalman Filter (UKF) has been used extensively for state estimation of battery models [6], [7]. In this paper, investigation is made into the practicality of combining existing state estimators with adaptive routines for online battery parameter tuning with the goal of tracking some of the aging effects that occur due to battery charge and discharge cycling. There is an ongoing need to update the battery model parameters as the battery ages. Present and past data collected during battery usage may provide information either in real-time or post operational to perform parameter updates, resulting in a battery model that will more accurately predict SoC. This in turn enables better predictions of the time of depletion, End of Discharge (EOD) and the closely related time remaining known as Remaining Useful Life (RUL).

2. Battery Model and Parameter Estimation

In this section the open circuit battery model is developed using a nonlinear equation that captures the near-equilibrium slow discharge and the open circuit voltage characteristics of the battery. The data set used to identify the equation coefficients is described in Appendix B, Figure B.1. Figure 1 shows the equivalent circuit model. The dashed arrows represent potential differences with the arrowhead at the assumed more positive potential. Here U_{oc} is the open

circuit voltage, *I(t)* is the discharge current, U_d is the total voltage across the resistor and resistor-capacitor pair, U_p is the voltage across the parallel resistor-capacitor pair, R_0 is the

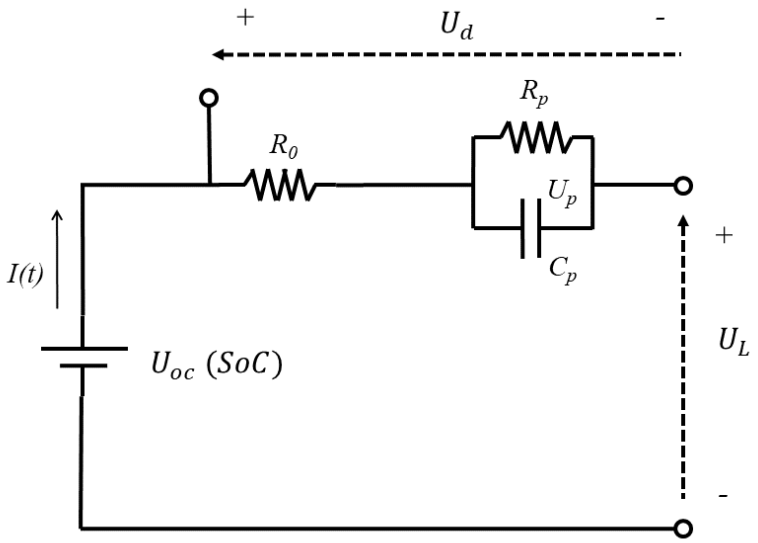

Figure 1 Equivalent Circuit Model

battery internal resistance, and U_L is the battery terminal voltage. The RC network characterizes the battery electrode polarization phenomenon.

2.1 Estimation of U_{oc}

For the equilibrium U_{oc} identification process, it is assumed that the resistors and capacitor do not play a significant role in modeling the battery behavior since the current draw is very low and electrode polarization effects may be neglected since the discharge is very slow and over a long time period. The equation for U_{oc} as a function of *SoC* S_t at time *t* is given in equation (1).

$$U_{oc,t}(S_t) = K_0 - K_1 S_t - {}^{K_2}/_{S_t} + K_3 \ln S_t + K_4 \ln(1 - S_t) \tag{1}$$

The data as described in Appendix B is used to fit the coefficients K_0 through K_4 to the battery discharge curve of Figure B.1. The resulting fit is shown in Figure 2 along with the parameter values presented in Table 1. As can be seen in Figure 2, equation (1) provides a close fit for the open circuit voltage U_{oc}. Using equation (1), the battery can be modeled during low current, slow discharge. However, for larger currents and faster discharge, additional equivalent circuit components must be added to account for battery behavior. The fit values shown in Table 1 were obtained using the Nelder-Mead method. Here the initial values were taken from [8]. It was assumed that the charge S_t started with the battery fully charged with $S_t = 1$ and that the battery was fully discharged with $S_t = 0$ at the end of the data set. However, equation (1) has singularities at these end points, so S_t was restricted to vary between 0.01 and 0.99.

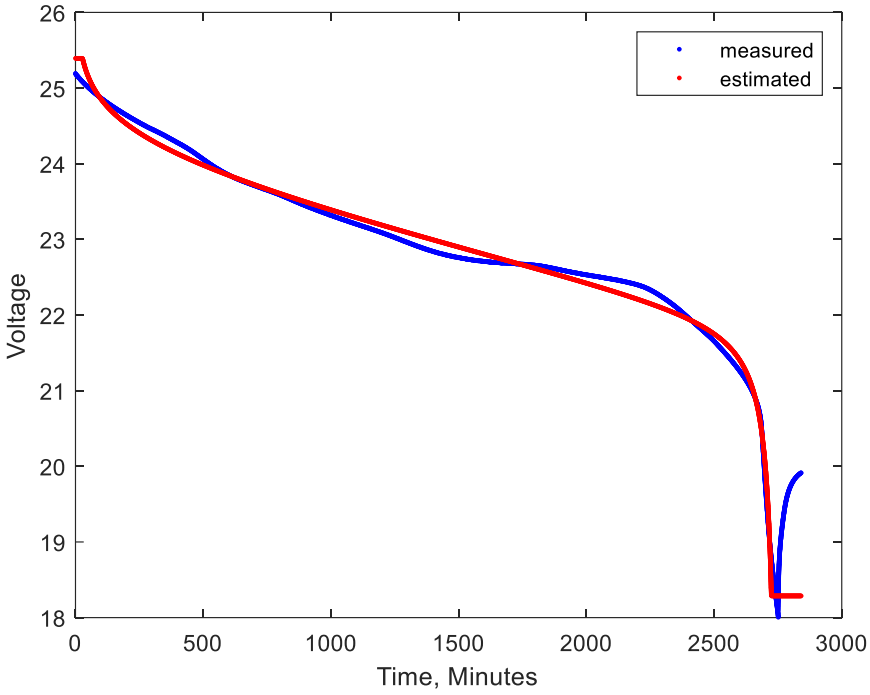

Figure 2 Plot of measured voltage and Uoc

Table 1 Equation (1) parameters

	Initial	Final
K_0	25.960	21.9696
K_1	-1.4346	-1.7180
K_2	0.0450	0.0368
K_3	-0.4602	0.0043
K_4	-0.0043	-0.3821

2.2 Estimation of U_d Components Using RLS

In this section the values of R_0, R_p, and C_p are estimated using Recursive Least Squares, RLS [9]. RLS is like batch least squares but updates parameter estimates as data becomes available. Since the circuit producing U_d of Figure 1 is linear, linear techniques such as RLS may be used. Using circuit theory, the equation for Figure 1 is first derived in continuous time. The discrete time model is then derived, and the transfer function is used to find expressions for the component values.

Consider the circuit shown in Figure 1. Using Kirchhoff's voltage and current laws, the equation for this circuit is shown in equation (2).

$$U_L(t) - U_{oc}(S_t) + R_0 I(t) + U_p(t) = 0 \tag{2}$$

$$I(t) = \frac{U_p(t)}{R_p} + C_p \frac{dU_p(t)}{dt}$$

Combining equation set (2) with the expression for S_t, the continuous time state equation may be written as shown in equation (3) where the time constant is $\tau = R_p C_p$.

$$\begin{bmatrix} \dot{S}_t \\ \dot{U}_p(t) \end{bmatrix} = \begin{bmatrix} 0 & 0 \\ 0 & -1/\tau \end{bmatrix} \begin{bmatrix} S_t \\ U_p(t) \end{bmatrix} + \begin{bmatrix} -1/C_{Max} \\ 1/C_p \end{bmatrix} I(t) \tag{3}$$

We convert equation (3) to discrete time as shown in equation (4) where T_s is the sample period and k is the time step. The output equation $U_L(k)$ is shown for completeness.

$$\begin{bmatrix} S(k) \\ U_p(k) \end{bmatrix} = \begin{bmatrix} 1 & 0 \\ 0 & e^{-T_s/\tau} \end{bmatrix} \begin{bmatrix} S(k-1) \\ U_p(k-1) \end{bmatrix} + \begin{bmatrix} -T_s/C_{Max} \\ R_p\left(1 - e^{-T_s/\tau}\right) \end{bmatrix} I(k) \tag{4}$$

$$U_L(k) = U_{oc}(S(k)) - U_p(k) - R_0 I(k)$$

$$U_{oc}(S(k)) = K_0 - K_1 S(k) - K_2/S(k) + K_3 \ln S(k) + K_4 \ln(1 - S(k))$$

The goal of the adaptive routine is to adjust the circuit parameters as data becomes available to closely match the battery behavior. To aid in the formulation of the adaptive routine, the Laplace transform is taken using Figure 1 and shown in equation (5). From the circuit equation, the transfer function *G(s)* is found. Here the output is the voltage developed across the circuit components, U_d, and the input is the current during discharge, *I(t)*. Polarities are as shown in Figure 1 and the symbol // means "parallel with."

$$U_L(s) - U_{oc}(s) + R_0 I(s) + R_p \;//\; (1/(C_p s))\, I(s) = 0 \tag{5}$$

$$G(s) \equiv \frac{U_d(s)}{I(s)} = \frac{U_{oc}(s) - U_L(s)}{I(s)} = R_0 + \frac{R_p}{1 + R_p C_p s}$$

Equation (5) needs to be expressed in the discrete time frequency domain. The bilinear transform is used here. The bilinear transform essentially uses the first order approximation and substitutes into the continuous time transfer function: $s \leftarrow \frac{2}{T_s}\frac{z-1}{z+1}$ where T_s is the sample period. After doing the substitution and performing algebraic manipulations, we get the discrete time transfer function of equation (6).

$$G(z) = R_0 + \frac{R_p}{1 + R_p C_p \frac{2}{T_s}\left(\frac{z-1}{z+1}\right)} = \frac{a_2 + a_3 z^{-1}}{1 + a_1 z^{-1}} \tag{6}$$

$$a_1 = \frac{T_s - 2R_p C_p}{T_s + 2R_p C_p} \quad a_2 = \frac{R_0 T_s + R_p T_s + 2R_0 R_p C_p}{T_s + 2R_p C_p} \; a_3 = \frac{R_0 T_s + R_p T_s - 2R_0 R_p C_p}{T_s + 2R_p C_p}$$

The values $a_1, a_2,$ and a_3 are solved for using RLS. To do this, the inverse z transform is used to express the relationship between the voltage $U_d(k)$ and the current $I(k)$ as shown in equation (7).

$$G(z) = \frac{U_d(z)}{I(z)} = \frac{U_{oc}(z) - U_L(z)}{I(z)} = \frac{a_2 + a_3 z^{-1}}{1 + a_1 z^{-1}} \tag{7}$$

$$U_d(k) = -a_1 U_d(k-1) + a_2 I(k) + a_3 I(k-1)$$

We can now define the needed vectors for the RLS algorithm as shown in equation (8). Here the error for updating the parameter estimates *err(k)* is computed based on the difference of measured battery terminal voltage U_L and the estimated open circuit voltage $U_{oc}(k)$ minus the estimate $\widetilde{U}_d(k)$.

$$\theta = [a_1 \quad a_2 \quad a_3]^T \tag{8}$$

$$\phi = [-\widetilde{U}_d(k-1) \quad I(k) \quad I(k-1)]$$

$$\widetilde{U}_d(k) = \phi\theta$$

$$err(k) = U_d(k) - \widetilde{U}_d(k) = U_{oc}(k) - U_L(k) - \widetilde{U}_d(k)$$

The recursive least squares estimate for θ is shown in equation set (9). Here λ is the forgetting factor set to 0.97, *P* is the correlation matrix initialized to one across the diagonal and zero elsewhere, and θ was initialized to zero.

$$L = \frac{P\phi^T}{\lambda + \phi P \phi^T} \tag{9}$$

$$P = (P - L\phi P)/\lambda$$

$$\theta(k+1) = \theta(k) + L(err(k))$$

The RLS routine was applied to data set two as shown in Figure B.3. This data set was chosen because it exercises the battery the most due to the variations in current draw. Results are shown in Figures 3 through 7. The average value for each parameter was found by averaging the values after one hundred seconds, giving the adaptive routine time to settle.

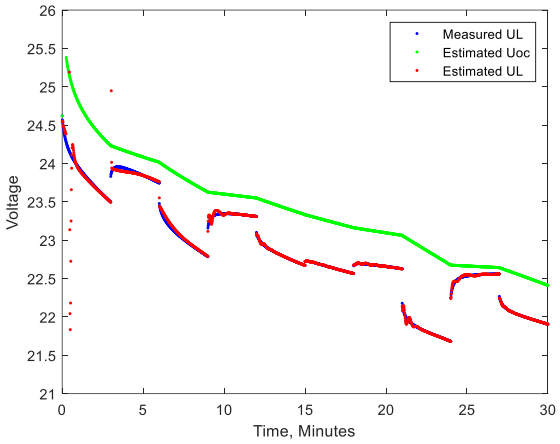

Figure 3 Load Voltage UL

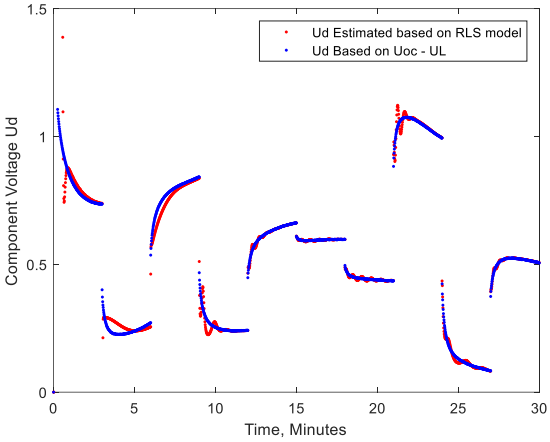

Figure 4 Component Voltage Ud

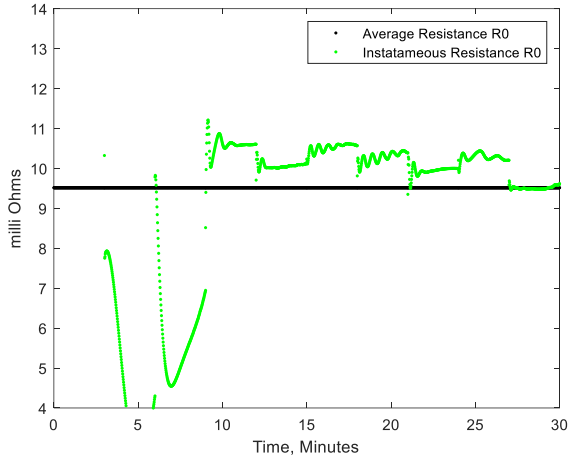

Figure 5 Internal Resistance R0

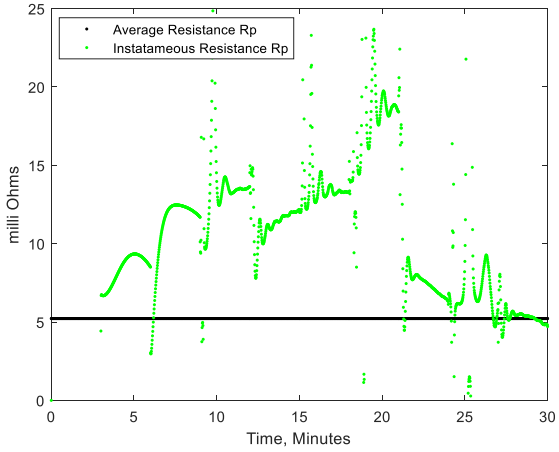

Figure 6 Polarization Resistance Rp

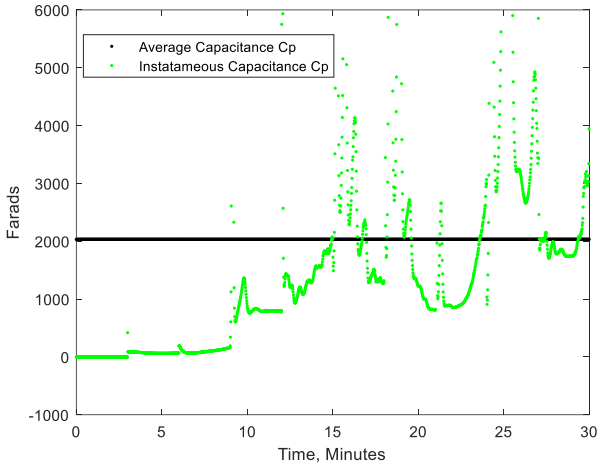

Figure 7 Polarization Capacitance Cp

In Figure 3 we see the battery terminal voltage and estimates, U_L. Here we see that the estimated terminal voltage and measured terminal voltage closely match as one would expect during system identification. The voltage U_{oc} is the open circuit voltage. That this value is larger and does not reflect the load variations during discharge is not surprising since for U_{oc} the battery internal resistance and polarization effects are taken to be zero; that is, unmodeled. Figure 4 shows the component voltage U_d. Here we see a close fit between the constructed measured voltage (the difference between the terminal voltage and U_{oc}) and the estimated component values based on the estimates of R_0, R_p, and C_p. The plots shown in Figures 5, 6, and 7 are the values for R_0, R_p, and C_p as the RLS routine adjusts during adaptation. The black line shown in each plot is the average value after one hundred seconds. Convergence can be seen in these plots to reasonable component values [8]. Once the RLS routine has developed estimates for a_1, a_2, and a_3, the component values may be obtained by solving equation set (6) for R_0, R_p, and C_p. The result is shown in equation set (10).

$$R_0 = \frac{(a_2 - a_3)}{1 - a_1} \tag{10}$$

$$\tau = \frac{T_s(1 - a_1)}{2a_1 + 2}$$

$$R_p = \left(1 + \frac{2\tau}{T_s}\right) a_2 - R_0 - \frac{2R_0\tau}{T_s}$$

$$C_p = \frac{\tau}{R_p}$$

3. State Estimation

In this section, state estimation is presented. For a given battery model, the state may be estimated in real-time as input/output data becomes available. State estimation may be

performed as model adaptation takes place, or the estimated state may be extended to include adaptation of selected model parameters [2]. Here, we investigate state estimation first in the fixed parameter model after convergence of the RLS solution. State estimation is developed for the Extended Kalman Filter, EKF, first followed by the Unscented Kalman Filter, UKF. These two estimators are chosen due to their applicability to nonlinear systems. State observability is addressed in Appendix C.

3.1 Extended Kalman Filter

The EKF requires that we determine the Jacobians of the state and output equations [2]. From equation (4), we can determine the needed expressions as shown in equation (11) where *f* is the set of state equations, *h* is the output equation, and *x* is the state.

$$F = \frac{\partial f}{\partial x} = \begin{bmatrix} \frac{\partial f_1}{\partial x_1} & \frac{\partial f_1}{\partial x_2} \\ \frac{\partial f_2}{\partial x_1} & \frac{\partial f_2}{\partial x_2} \end{bmatrix} = \begin{bmatrix} 1 & 0 \\ 0 & e^{-T_s/\tau} \end{bmatrix} \tag{11}$$

$$H = \frac{\delta h}{\delta x} = \begin{bmatrix} \frac{\delta h}{\delta x_1} & \frac{\delta h}{\delta x_2} \end{bmatrix} = \begin{bmatrix} -K_1 + \frac{K_2}{S^2(k)} + \frac{K_3}{S(k)} - \frac{K_4}{1 - S(k)} & -1 \end{bmatrix}$$

The EKF may be implemented using the equations for *F* and *H*.

Prediction (Time Update)

$$\tilde{x}(k) = f(\tilde{x}(k-1), I(k)) \tag{12}$$

$$P = FPF^T + Q$$

$$\tilde{U}_L(k) = h(\tilde{x}(k))$$

Update (Measurement)

$$\tilde{x}(k) = \tilde{x}(k) + PH^T(HPH^T + R)^{-1}\left(U_L(k) - \tilde{U}_L(k)\right)$$

$$P = P - PH^T(HPH^T + R)^{-1}HP$$

Equation set (12) may be used to estimate the state *x* for the given battery model. Here we have voltage measurements $U_L(k)$, estimated voltages $\tilde{U}_L(k)$, system process noise covariance *Q,* measurement noise *R,* and state covariance *P*. Good performance was observed with *Q* set to the identity matrix and *R* set to 25.

The observed state is the state of charge SoC and the parallel voltage U_p as given in Figure 1. These voltages are shown in Figure 10 and Figure 9 respectively. The voltage U_d shown in Figure 8 is the difference between the measured battery terminal voltage and the open circuit voltage $U_{oc.}$ Figure 11 is the battery terminal voltage. As can be seen from these figures, the observer tracks the states well and the difference between the estimated and measured battery output voltage is minimized as can be seen in Figure 11. Also shown in Figure 11 is the model voltage estimates without the observer.

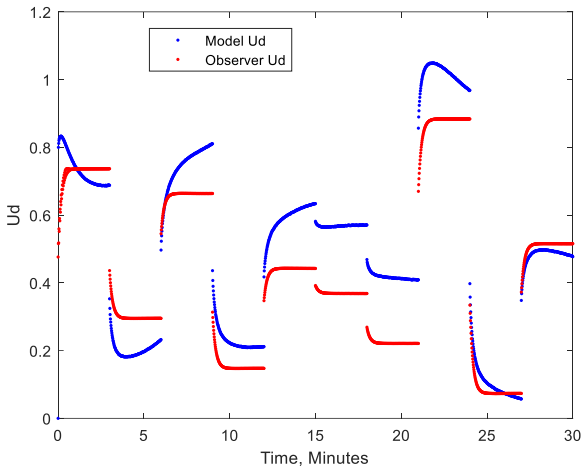

Figure 8 Voltage difference

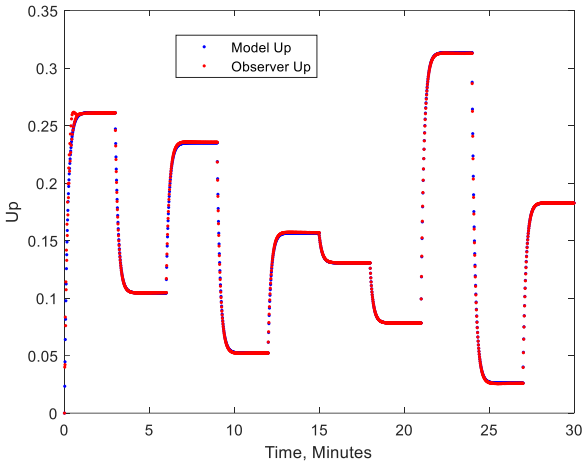

Figure 9 Voltage across parallel components

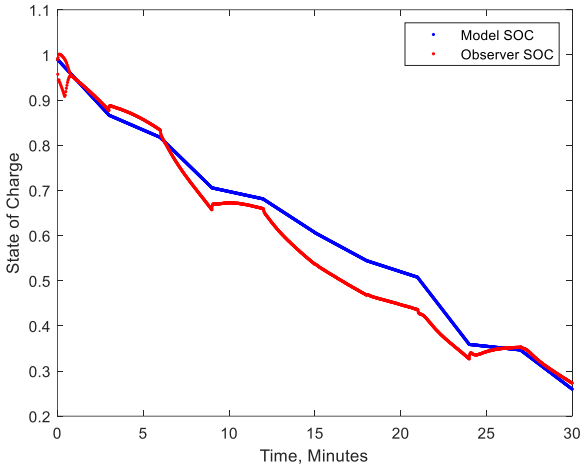

Figure 10 State of Charge

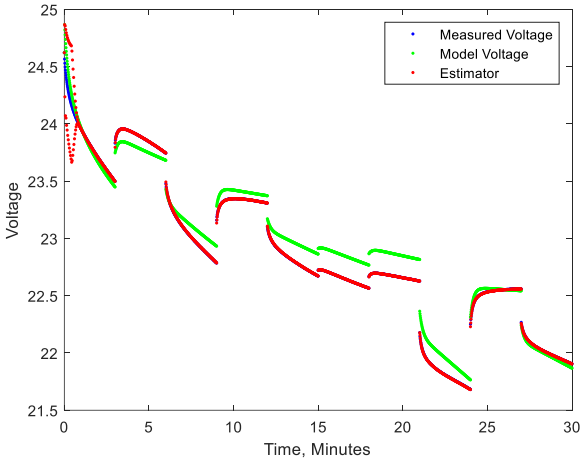

Figure 11 Terminal voltage UL

3.2 Unscented Kalman Filter

In this section the Unscented Kalman Filter (UKF) is developed for state estimation. The UKF is presented in equation set (13). A derivation of the unscented transform is presented in Appendix A.

The Unscented Kalman Filter is used for nonlinear state estimation. The equations are given below and can be found in reference [7]. First, the weights *w* and sigma points χ are calculated. Here n_x is the system order, κ is a tuning constant, $\hat{x}$ is the mean, and P_{xx} is the state autocorrelation. The superscript *i* is the i^{th} matrix column.

$$w^0 = \frac{\kappa}{n_x + \kappa}$$

$$w^i = \frac{1}{2(n_x + \kappa)}, \qquad i = 1,2, \dots, 2n_x$$

$$\chi^0 = \hat{x}_{k-1|k-1}$$

$$\chi^i = \hat{x}_{k-1|k-1} + \left(\sqrt{(n_x + \kappa)P_{k-1|k-1}}\right)^i, \qquad i = 1,2, \dots, n_x$$

$$\chi^i = \hat{x}_{k-1|k-1} - \left(\sqrt{(n_x + \kappa)P_{k-1|k-1}}\right)^i, \qquad i = n_x + 1, n_x + 2, \dots, 2n_x$$

The prediction step involves passing the sigma points through the nonlinear system model. The state equation is $f(\cdot)$ and the measurement equation is $g(\cdot)$. Both the state and measurement equations are determined from the equivalent circuit model of equation set (2). The input is the battery current $I(k)$ and *k* is the current time step. The output *y* is the measured load voltage.

$$\hat{\chi}^i = f\left(\chi^i, I(k)\right), \qquad i = 1,2, \dots, n_s$$

$$\hat{Y}^i = g(\chi^i), \qquad i = 1,2, \dots, n_s$$

$$\hat{x} = \sum_i^{n_s} w^i \hat{\chi}^i$$

$$\hat{y}_{k|k-1} = \sum_i^{n_s} w^i \hat{Y}^i$$

$$P_{k|k-1} = Q + \sum_i^{n_s} w^i \left(\hat{\chi}^i - \hat{x}_{k|k-1}\right)\left(\hat{\chi}^i - \hat{x}_{k|k-1}\right)^T$$

The update steps are shown below; n_s is the number of sigma points. The subscript notation $k|k-1$ means the current time step *k* given measurement data up to time $k-1$. The update occurs by using the new voltage measurement $y_k = U_L$ to update the state estimate.

$$P_{yy} = R + \sum_i^{n_s} w^i \left(\hat{Y}^i - \hat{y}_{k|k-1}\right)\left(\hat{Y}^i - \hat{y}_{k|k-1}\right)^T$$

$$P_{xy} = \sum_i^{n_s} w^i \left(\hat{\chi}^i - \hat{x}_{k|k-1}\right)\left(\hat{Y}^i - \hat{y}_{k|k-1}\right)^T$$

$$K_k = P_{xy} P_{yy}^{-1}$$

$$\hat{x}_{k|k} = \hat{x}_{k|k-1} + K_k\left(y_k - \hat{y}_{k|k-1}\right)$$

$$P_{k|k} = P_{k|k-1} - K_k P_{yy} K_k^T \tag{13}$$

In the above algorithm, Q is the process noise covariance matrix and R is the measurement noise covariance matrix. As with the EKF, the UKF may be used to estimate the states SoC and U_d. The results are shown in Figures 12-14.

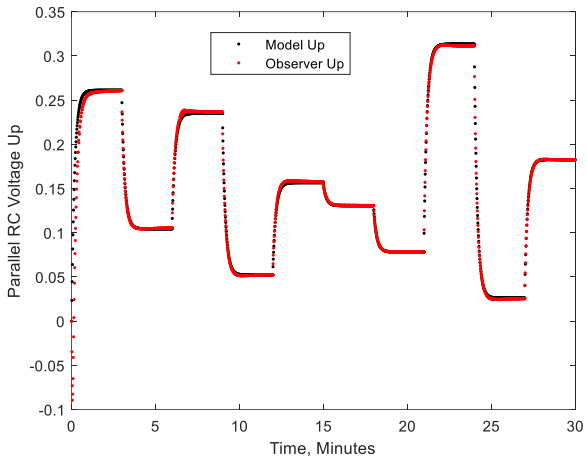

Figure 12 Voltage across parallel components

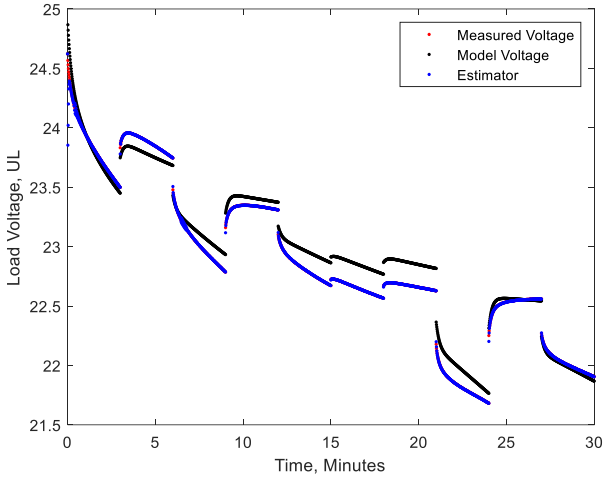

Figure 13 Terminal voltage UL

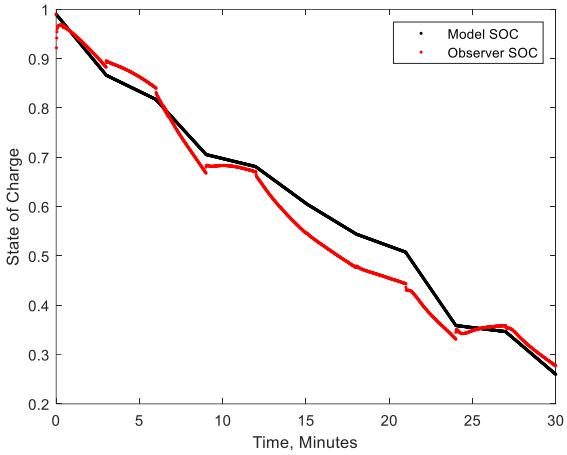

Figure 14 State of Charge

4. Combined Parameter Adaptation and State Estimation

In this section the real-time RLS routine will be combined with the EKF state observer to form the adaptive battery model. The EKF is chosen over the UKF in order to avoid the potential problem in computing the matrix square root. When combining the RLS with the EKF, the battery parameter values are updated first and then the updated model is used for EKF state estimation. The results are shown in Figures 15-18 where the variables are as previously defined.

It was observed that with both the system identification and state estimation occurring at the same time, a stable realization was rarely achievable for the data set used in this

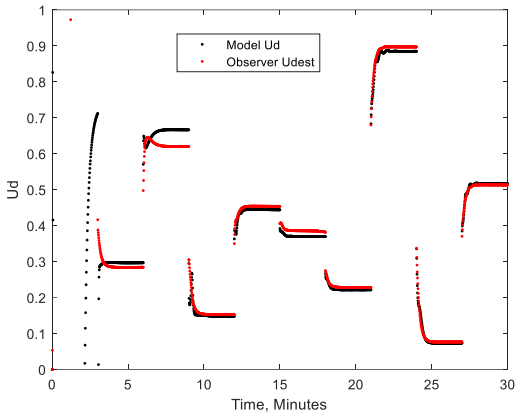

Figure 15 Voltage difference

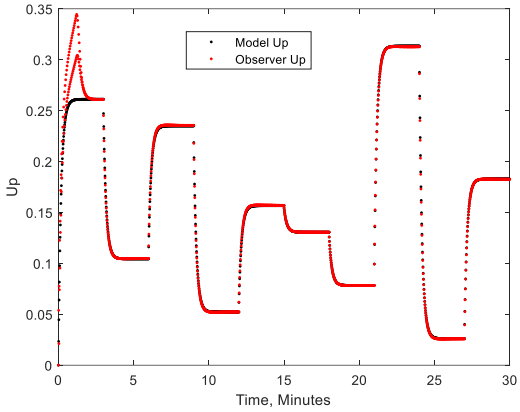

Figure 16 Voltage across parallel components

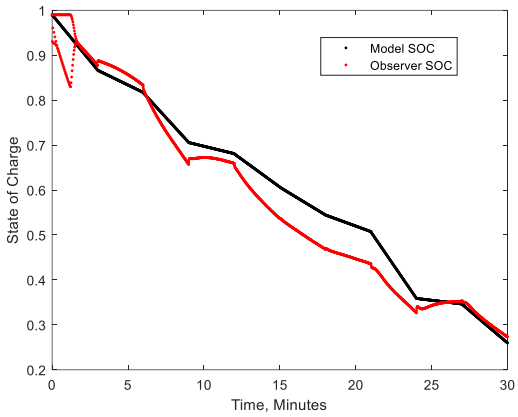

Figure 17 State of Charge

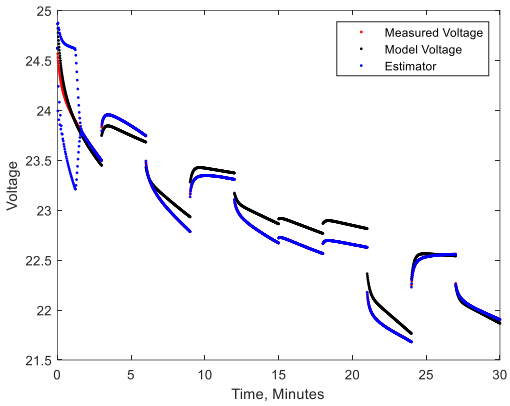

Figure 18 Terminal voltage U_L

implementation. This is most likely due to too many variations occurring at the same time with uncertainty in both the system state and model parameters. To resolve this, the system identification was performed first followed by state estimation once a stable model was identified. For linear systems with persistence excitation across the frequency domain of interest, model identification and state estimation are possible given that observability and controllability conditions are met. However, battery models are inherently nonlinear and for the implementation considered persistent system excitation for both model parameter identification and state identification was probably not achieved.

5. Conclusions

Nonlinear models must be used to accurately capture battery discharge behavior. The parameters for these models are time varying due to aging and environmental effects such as temperature and discharge history, making adaptive routines possible candidates for modeling these characteristics. However, due to the nonlinearity and possible instability of the battery models, adaptive routines often behave in unpredictable ways which make them of limited use for real world implementation. One possible solution would be to use supervised updates and constrain the range of parameter variation. By using a supervisor to govern updates and place bounds on parameter and state estimate variation it may be possible to update battery parameters to account for environmental and aging effects. This would only be possible if system excitation was sufficiently frequency-rich to capture variations in the dynamical

response, which will occur if the current draw from the battery has enough signal content to excite the battery internal dynamics. A possible future use of adaptive routines might be found in offline battery model identification. Here a battery cycler may be used to charge/discharge the battery in a temperature-controlled environment. With this arrangement, the battery dynamics would be properly excited making model parameter identification possible and containing the impact of model instability on mission objectives.

References

[1] M. S. Grewal and A. P. Andrews, "Applications of Kalman Filtering in Aerospace 1960 to the Present," *IEEE Control Systems Magazine,* vol. 30, no. 3, pp. 69-78, June 2010.

[2] G. L. Plett, "Extended Kalman filtering for battery management systems of LiPB-based HEV battery packs, Part 1. Background, Part 2. Modeling and identification, Part 3. State and parameter estimation," *Journal of Power Sources,* vol. 134, pp. 252-261, 2004.

[3] M. Daigle and S. Sankararaman, "Predicting Remaining Driving Time and Distance of a Planetary Rover under Uncertainty," *ASCE-ASME J. Risk and Uncertainty in Engineering Systems, Part B: Mech. Engineering,* vol. 2, no. DO - 10.1115/1.4032848, 2016.

[4] M. Daigle, "Prognostics model library [computer software]," NASA, 2016. [Online]. Available: https://github.com/nasa/PrognosticsModelLibrary. [Accessed 2 September 2020].

[5] W. Yebin, H. Fang, L. Zhou and T. Wada, "Revisiting the State-of-Charge Estimation for Lithium-Ion Batteries, A Methodical Investigation of the Extended Kalman Filter Approach," *IEEE Control Systems Magazine,* Vols. 1066-033X, no. August, pp. 73-96, 2017.

[6] M. Daigle, "End-of-discharge and End-of-life Prediction in Lithium-ion Batteries with Electrochemistry-based Aging Models," in *American Institute of Aeronautics and Astronautics*, San Diego, 2016.

[7] S. J. Julier and J. K. Uhlmann, "A new extension of the kalman filter to nonlinear systems," in *AeroSense: The 11th International Symposium on Aerospace/Defence Sensing, Simulation and Controls*, 1997.

[8] C. Jiang, S. Wang, B. Wu, B. Etse-Dabu and X. Xiong, "A Novel Adaptive Extended Kalman Filtering and Electrochemical-Circuit Combined Modeling Method for the Online Ternary Battery state-of-charge Estimation," *Int. J. Electrochem. Sci.,* vol. 15, no. 10.20964, p. 9720 – 9733, 2020.

[9] K. J. Astrom and B. Wittenmark, Adaptive Control, Reading, Massachusetts: Addison-Wesley Publishing Company, 1995.

[10] S. Särkkä, Bayesian Filtering and Smoothing, New York: Cambridge University Press, 2013.

[11] M. Daigle and C. S. Kulkarni, "Electrochemistry-based Battery Modeling for Prognostics," in *Annual Conference of the Prognostics and Health Management Society*, New Orleans, 2013.

[12] D. Karthikeyan, G. Sikha and R. White, "Thermodynamic Model Development for Lithium Intercalation Electrodes," *Journal of Power Sources,* vol. 185, no. 2, pp. 1398-1407, 2008.

[13] T. R. B. Grandjean, A. McGordon and P. A. Jennings, "Structural Identifiability of Equivalent Circuit Models for Li-Ion Batteries," *Energies,* vol. 10, no. 90, pp. 45-46, 2017.

[14] Shenzhen Grepow Battery Co., LTD, "https://community.openppg.com/ Material Safety Data Sheet Report No.: 17PNS01051 07001," 17 January 2017. [Online]. Available: https://community.openppg.com/uploads/short-url/yfEcb9SBzbTDBGCPTgdqwXu9rOU.pdf. [Accessed 2 September 2020].

Appendix A

The purpose of this appendix is to give the reader a sense of the development of the Unscented Kalman Filter, UKF. Presented here is the basic general Gaussian filter with descriptions of both quadrature and cubature integration used in implementing the UKF [10]. While the provided explanations do not serve as mathematical proofs, they do give the reader a sense for how the various methods were developed along with applications.

The system model is assumed to be nonlinear and Markovian. Here we have that

$$x_k = f(x_{k-1}) + q_{k-1}$$

$$y_k = h(x_{k-1}) + r_k$$

where q_{k-1} and r_k are independent Gaussian noise. The variable *k* is the time step and $f(\cdot)$ and $h(\cdot)$ are nonlinear transforms. The measurement at *k* is y_k and the *n* dimensional state to be estimated is x_k. It is the goal of the Bayesian filter to return state estimates given past output measures. The state and measurement probability density functions may be expressed as

$$x_k \sim p(x_k|x_{k-1})$$

$$y_k \sim p(y_k|x_k)$$

The Bayesian filter estimates the state density given all past measurements up to *k*; that is estimate $p(x_k|y_{1:k})$. Per Bayes' rule, we may write the probability density function conditioned on $y_{1:k-1}$ as follows

$$p(x_k|y_k, y_{1:k-1}) = \frac{p(y_k|x_k, y_{1:k-1})p(x_k|y_{1:k-1})}{p(y_k|y_{1:k-1})}$$

Because of the Markovian assumption and application of the Chapman-Kolmogorov equation to the denominator, we may write

$$p(x_k|y_{1:k}) = \frac{p(y_k|x_k)p(x_k|y_{1:k-1})}{\int p(y_k|x_k)p(x_k|y_{1:k-1})dx_k}$$

The above expression may be used in the Bayesian filter algorithm. The filter consists of three basic steps: initialization, prediction, and update. We start with some initial estimate of the state density to be estimated $p(x_0)$. Given measurements up to and including time step *k*-1, we can predict state x_k before measurement y_k with the Chapman-Kolmogorov equation

$$p(x_k|y_{1:k-1}) = \int p(x_k|x_{k-1})p(x_{k-1}|y_{1:k-1})dx_{k-1}$$

To update the estimate at time step k, we use the measurement y_k and Bayes rule to evaluate $p(x_k|y_{1:k})$. In general, a closed form solution does not exist for the Bayesian filter. However, if both $f(\cdot)$ and $h(\cdot)$ are linear functions, the Kalman filter may be used.

To use the Bayesian filter for nonlinear state estimation, some assumptions and approximations must be made. First, we assume that the system output of the nonlinear transform is approximately Gaussian. In general, this is not the case; but the Gaussian approximation may provide a close enough fit to meet filtering requirements. There is also a need to solve integrals in real time that in general do not have closed form solutions. To do this, numerical solutions are used to approximate the integral. To lay out the filter algorithm, consider the following matrix relation for Gaussian random variables: $x \sim N(x|\mu, P)$ where *x* is a Gaussian vector with mean μ and covariance matrix *P*. The vector *x* can be partitioned into two sections.

$$x = \begin{bmatrix} x_a \\ x_b \end{bmatrix} \quad \mu = \begin{bmatrix} \mu_a \\ \mu_b \end{bmatrix} \quad P = \begin{bmatrix} P_a & P_c \\ P_c^T & P_b \end{bmatrix}$$

The conditional probabilities of the joint random variables x_a and x_b are given by

$$p(x_a|x_b) = N\left(x_a|\, \mu_a + P_c P_b^{-1}(x_b - \mu_b),\; P_a - P_c P_b^{-1} P_c^T\right)$$

$$p(x_b|x_a) = N(x_b|\, \mu_b + P_c^T P_a^{-1}(x_a - \mu_a),\; P_b - P_c^T P_a^{-1} P_c)$$

The above identity may be used to determine the Bayesian filter algorithm through moment matching. We can define the joint probability density function for x_k and y_k and next determine the conditional density of x_k given the new measure y_k has occurred in the update step. Using the templet above to stage our construction, we have the following.

$$p(x_k\, , y_k) = N(x|\mu\, , P) \qquad x = \begin{bmatrix} x_k \\ y_k \end{bmatrix} \quad \mu = \begin{bmatrix} m_k^- \\ \mu_k \end{bmatrix} \quad P = \begin{bmatrix} P_k^- & C_k \\ C_k^T & S_k \end{bmatrix}$$

$$p(x_k \mid y_k) \; = N(x_k|m_k\, , P_k)$$

$$m_k = m_k^- + C_k S_k^{-1}(y_k - \mu_k) \qquad P_k = P_k^- - C_k S_k^{-1} C_k^T$$

The algorithm is shown below for the case of additive noise and nonlinear system model $f(\cdot)$ and measurement model $h(\cdot)$.

Algorithm for General Gaussian Filter

Prediction: We first need to predict the mean and covariance of the state x_k before a measurement occurs. We do this by using the state model along with our best estimate of the density function, assumed to be Gaussian. Of the mean and covariance, we have

$$m_k^- = \int f(x_{k-1}) N(x_{k-1} | m_{k-1}, P_{k-1}) dx_{k-1}$$

$$P_k^- = \int \{f(x_{k-1}) - m_k^-\}\{f(x_{k-1}) - m_k^-\}^T N(x_{k-1} | m_{k-1}, P_{k-1}) dx_{k-1} + Q_{k-1}$$

Update: To update our estimate of the state x_k given the recent measurement y_k, we use the conditional density relationship $p(x_k \mid y_k)$ as derived above using moment matching as well as the definitions of mean and covariance for a random variable given its probability density function. We assume a Gaussian distribution. Although in general the output of a nonlinear system given a Gaussian input is not Gaussian, we make this assumption as an approximation to design a filter realizable in real time.

$$\mu_k = \int h(x_k) N(x_k |\, m_k^-,\, P_k^-) dx_k$$

$$S_k = \int \{h(x_k) - \mu_k\}\{h(x_k) - \mu_k\}^T N(x_k |\, m_k^-,\, P_k^-)\, dx_{k-1} + R_k$$

$$C_k = \int (x_k - m_k^-)\{h(x_k) - \mu_k\}^T N(x_k |\, m_k^-,\, P_k^-)\, dx_{k-1} + R_k$$

With solutions to the above integrals, we can finish the recursion using the results from moment matching.

$$m_k = m_k^- + C_k S_k^{-1}(y_k - \mu_k) \qquad P_k = P_k^- - C_k S_k^{-1} C_k^T$$

In general, closed form solutions to the integrals are not possible. Numerical integration techniques are used to approximate the integrals for real time implementation. Two techniques are considered here: Gauss-Hermite and Spherical cubature.

For Gauss-Hermite integration, consider the definition of the mean given that x is a Gaussian random vector and $g(\cdot)$ is some transform.

$$\int g(x) N(x|m, P) dx = \frac{1}{(2\pi)^{n/2}|P|^{1/2}} \int g(x) exp\left\{-\frac{1}{2}(x-m)^T P^{-1}(x-m)\right\} dx$$

To use Gauss-Hermite integration, we must use a change of variables to make the distribution zero mean and unit covariance. Let $x = m + \sqrt{P}\xi$ and recalling that we must take the determinant of the Jacobean for multivariable change of variables we have

$$\frac{1}{(2\pi)^{n/2}|P|^{1/2}} \int g\big(m + \sqrt{P}\xi\big) exp\left\{-\frac{1}{2}\big(m + \sqrt{P}\xi - m\big)^T P^{-1}\big(m + \sqrt{P}\xi - m\big)\right\} \big|\sqrt{P}\big| d\xi$$

Since the covariance matrix is positive semi-definite, we have $\big|\sqrt{P}\big| = |P|^{1/2}$. We now have the desired form.

$$\int g(x)N(x|m,P)dx = \int g\left(m+\sqrt{P}\xi\right)N(\xi|0,I)d\xi$$

One way to approximate this integral is to use Hermite polynomials. This approximation comes from the mathematics and physics communities and is simply stated here without derivation.

$$\int g(x)N(x|m,P)dx \approx \sum_{i_1,\ldots,i_n} W_{i_1,\ldots,i_n} g\left(m+\sqrt{P}\xi^{(i_1,\ldots i_n)}\right)$$

The sigma points ξ are the roots of the p^{th} order Hermite polynomial and the weights *W* are given by

$$W_{i_1,\ldots i_n} = \frac{p!}{p^2\left\{H_{p-1}\xi^{i_1}\right\}^2} \times \ldots \times \frac{p!}{p^2\left\{H_{p-1}\xi^{i_n}\right\}^2}$$

Since this integration method takes an *n* dimensional integral and breaks it down to *n* one dimensional integrals, the number of sigma points grows on order p^n.

To reduce the computational burden of numerical iteration, spherical cubature integration is used. The algorithm is presented here without development.

Consider the *2n*-point approximation to the multi-dimensional Gaussian integral

$$\int \mathbf{g}(\boldsymbol{\xi})N(\boldsymbol{\xi} \mid \mathbf{0}, \boldsymbol{I})d\boldsymbol{\xi} \approx W\sum_{i=1}^{2n} g\left(c\boldsymbol{u}^{(i)}\right)$$

Here *W* and *c* are scalar constants to be determined. There are *2n* symmetric vectors, each of length *n*. As an example, consider the case for $n = 3$.

$$u = \left\{u^{(1)}, u^{(2)}, u^{(3)}, u^{(4)}, u^{(5)}, u^{(6)}\right\} = \left\{\begin{bmatrix}1\\0\\0\end{bmatrix}, \begin{bmatrix}0\\1\\0\end{bmatrix}, \begin{bmatrix}0\\0\\1\end{bmatrix}, \begin{bmatrix}-1\\0\\0\end{bmatrix}, \begin{bmatrix}0\\-1\\0\end{bmatrix}, \begin{bmatrix}0\\0\\-1\end{bmatrix}\right\}$$

We can determine the constants W and c by considering two exact solutions; one for $g_j(\boldsymbol{\xi}) = 1$ and one for $g_j(\boldsymbol{\xi}) = \xi_j^2$. The subscript *j* here is for the j^{th} element of a given vector from the set of *2n* vector set *u*. For the case of $g_j(\boldsymbol{\xi}) = 1$ we have that

$$\int (1)N(\boldsymbol{\xi} \mid \mathbf{0}, \boldsymbol{I})d\boldsymbol{\xi} = 1 = W\sum_{i=1}^{2n} 1 = W2n \qquad W = \frac{1}{2n}$$

For the case of $g_j(\boldsymbol{\xi}) = \xi_j^2$ we have that

$$\int \xi_j^2 N(\boldsymbol{\xi} \mid \mathbf{0}, \boldsymbol{I})d\boldsymbol{\xi} = 1 = W\sum_{i=1}^{2n} \left\{cu_j^{(i)}\right\}^2 = W2c^2 \qquad c = \sqrt{n}$$

For example, consider the case of $n = 3$ as described above. If we choose the second element, for example, we can write

$$W\sum_{i=1}^{2n}\left\{cu_2^{(i)}\right\}^2 = W\{c^2 0^2 + c^2 1^2 + c^2 0^2 + c^2 0^2 + c^2(-1)^2 + c^2 0^2\} = W2c^2 = \frac{1}{2n}2c^2 \quad c = \sqrt{n}$$

As we did with Gauss-Hermite integration, we can do a change of variables to generalize the spherical cubature integration.

$$\int g(\boldsymbol{x})N(\boldsymbol{x}|\boldsymbol{m},\boldsymbol{P})dx \approx \frac{1}{2n}\sum_{i=1}^{2n} g\left(\boldsymbol{m} + \sqrt{\boldsymbol{P}}\boldsymbol{\xi}^{(i)}\right) \quad \boldsymbol{\xi}^{(i)} = \sqrt{n}\boldsymbol{u_i}$$

The approximation above is very like the unscented transform. If we include a zero-vector sigma point and an additional parameter for tuning, we can obtain the unscented transform.

By using either the Gauss-Hermite or spherical cubature integration to solve the integrals of the Kalman filter algorithm, one obtains a realizable implementation for nonlinear state estimation.

Appendix B

This appendix describes the battery data used for parameter identification and modeling analysis. Four data sets were created using a Maccor 4000 battery cycler. The first data set was found to have corrupted data and data set two is presented in Figure B.1, Figure B.2, and Figure B.3. In these figures blue is the battery voltage and red the current. Data set two is presented here because it is the one used in the battery model simulations. For the flight data, battery four was used.

The red lines in the figures are the current values labeled on the right axis. For the slow discharge, the current was held at around 0.44 amperes; for the 1 C discharge the current was held around 22 amperes, and for the variable discharge case the current went through quantized steps as can be seen in the red line shown in Figure B.3.

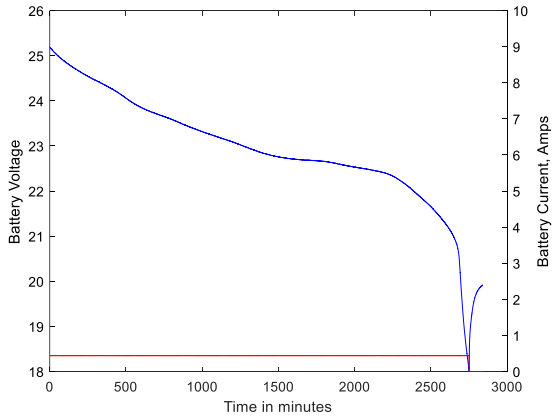

Figure B.1. Slow Discharge.

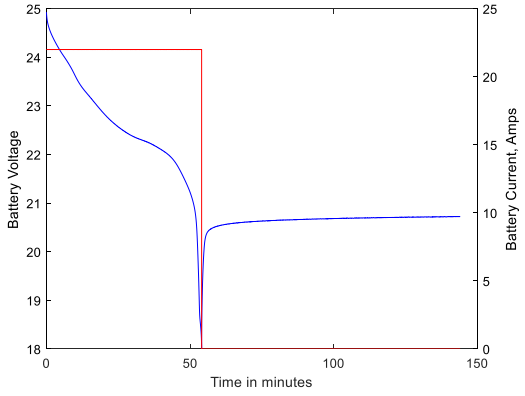

Figure B.2. One-C Discharge.

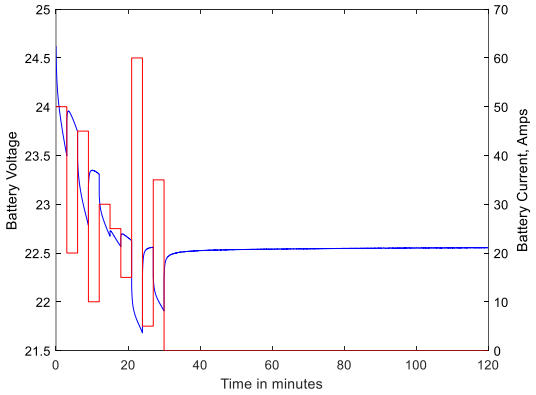

Figure B.3. Variable Discharge.

Appendix C

The purpose of this appendix is to investigate observability of the battery model. Observability for this nonlinear system is demonstrated by forming the observability coordinates, taking the Jacobean of the observability coordinates to form the observability matrix, and finally computing the condition number of the observability matrix to check for observability. Consider the continuous time battery model for Figure 1 shown below.

$$\dot{x} = f(x) = \begin{bmatrix} \dot{S}_t \\ \dot{U}_p(t) \end{bmatrix} = \begin{bmatrix} -I(t)/C_{Max} \\ -U_p(t)/\tau + I(t)/C_p \end{bmatrix} = \begin{bmatrix} 0 & 0 \\ 0 & -1/\tau \end{bmatrix} \begin{bmatrix} S_t \\ U_p(t) \end{bmatrix} + \begin{bmatrix} -1/C_{Max} \\ 1/C_p \end{bmatrix} I(t)$$

$$y = h(x) = U_L(t) = K_0 - K_1 S_t - K_2/S_t + K_3 \ln S_t + K_4 \ln(1 - S_t) - U_p(t) - R_0 I(t)$$

In the above equation the state is x with state transition $f(x)$ and output function $y = h(x) = U_L(t)$ which is the battery output voltage. Recall that the Lie derivative is defined as $L_f h(x) = \left(\partial h(x)/\partial x\right) f(x)$ and the observability coordinates are $[y \quad L_f y]^T$.

$$\begin{bmatrix} y \\ L_f y \end{bmatrix} = \begin{bmatrix} K_0 - K_1 S_t - K_2/S_t + K_3 \ln S_t + K_4 \ln(1 - S_t) - U_p(t) - R_0 I(t) \\ \left(\frac{-I(t)}{C_{Max}}\right)\left(-K_1 + \frac{K_2}{S_t^2} + \frac{K_3}{S_t} - \frac{K_4}{1 - S_t}\right) + \frac{U_p(t)}{\tau} - \frac{I(t)}{C_p} \end{bmatrix}$$

The observability matrix is found by taking the Jacobean of the observability coordinates as shown below.

$$Obv = \nabla \begin{bmatrix} y \\ L_f y \end{bmatrix} = \begin{bmatrix} \partial y/\partial x_1 & \partial y/\partial x_2 \\ \partial L_f y/\partial x_1 & \partial L_f y/\partial x_2 \end{bmatrix}$$

$$Obv = \begin{bmatrix} -K_1 + \frac{K_2}{S_t^2} + \frac{K_3}{S_t} - \frac{K_4}{1 - S_t} & -1 \\ \left(\frac{I(t)}{C_{Max}}\right)\left(\frac{2K_2}{S_t^3} + \frac{K_3}{S_t^2} + \frac{K_4}{(1 - S_t)^2}\right) & \frac{1}{\tau} \end{bmatrix}$$

To investigate observability, the condition number of the observability matrix is found. The condition number is the ratio of the largest singular value of Obv to the smallest. A plot of the condition number along with the current is shown in Figure C.1 below. From this figure we see that the maximum condition number is around one thousand, indicating that there is no problem with observability for the given model and current profile. Note that observability is maintained even with the current draw drops to zero for this battery model.

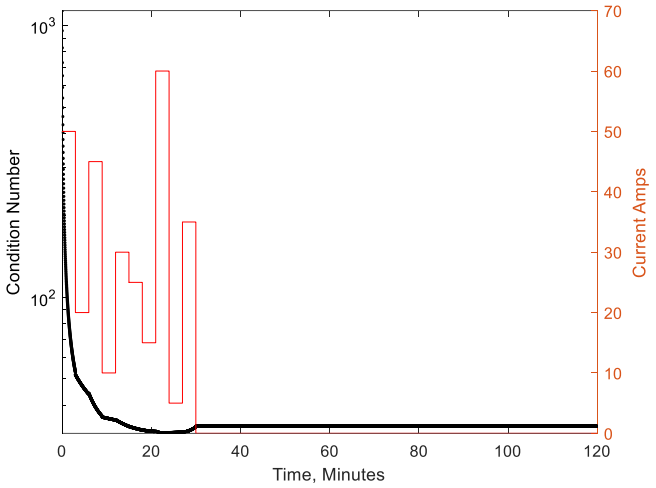

Figure C.1 Plot of condition number, black, and current, red